Size Effects in the Thermal Conductivity of Amorphous Polymers

Tianli Feng,[1,*] Jixiong He,[2] Amit Rai,[1] Diana Hun,[1] Jun Liu,[2] and Som S. Shrestha[1,†]

[1] *Buildings and Transportation Science Division, Oak Ridge National Laboratory, Oak Ridge, Tennessee 37831, USA*

[2] *Department of Mechanical and Aerospace Engineering, North Carolina State University, Raleigh, North Carolina 27695, USA*

(Received 13 May 2020; revised 24 July 2020; accepted 31 August 2020; published 14 October 2020)

Manipulating thermal conductivity through nanoengineering is of critical importance to advance technologies, such as soft robotics, artificial skin, wearable electronics, batteries, thermal insulation, and thermoelectrics. Here, by examining amorphous polymers, including polystyrene, polypropylene, polyethylene, and ethylene vinyl alcohol, using molecular dynamics simulations, we find that the thermal conductivities of amorphous polymers can be reduced below their amorphous limit by size effects. Size-dependent thermal transport in amorphous materials is decomposed into crystalline, crystalline-to-amorphous, and amorphous regimes. In the amorphous regime, the mean free path of propagating heat carriers can range from tens of nanometers to more than 100 nm, contributing 16%–36% of the total thermal conductivity. A two-channel model that combines no size effect (i.e., difusons and locons) and size effect (i.e., propagons) is proposed to account for size-dependent thermal conductivity. We also find that the presence of charged molecules in polymers can significantly affect the thermal conductivity and its size effects due to electrostatic interactions. This work provides insights into the thermal conductivity of amorphous polymers that will have a broad impact on the nano- and chemical engineering of polymers for various energy-related applications.

DOI: 10.1103/PhysRevApplied.14.044023

I. INTRODUCTION

Polymers have shown great potential in various modern applications, such as soft robotics, organic electronics, three-dimensional printing, artificial skin, flexible and wearable electronics, battery electrolytes, thermal insulation, and thermoelectrics [1–10]. They offer many advantages compared with traditionally used metals and ceramics, such as lightweight, low cost, high corrosion resistance, nontoxicity, and convenient manufacturability. Among the physical properties, thermal conductivity (κ) is a crucial component that determines the energy efficiency of building enclosures, the efficacy of cold chain system for vaccines, thermal management effectiveness of robotics and electronics, safety of batteries, and efficiency of thermoelectrics. The ability to manipulate thermal transport in polymers is key to many future technology breakthroughs.

Theories of thermal transport have been well studied in crystalline materials in the past two decades [11–14]. The periodic arrangement of atoms in crystalline materials can form wavelike lattice vibrations, quantified as phonons, which propagate with certain wavelengths and speeds. Heat transport is dominated by phonons in crystals. Various phonon modes in a material can scatter (collide) with each other, and therefore, have a certain finite mean free path (MFP). While the material size is comparable with or smaller than some phonons' MFPs, these phonons can transport heat between boundaries within the material in a ballistic manner without scattering with other phonons. Such an effect is called the size effect, and those phonons are called ballistic phonons. Due to the size effect, phonon transport is limited by the material's boundaries, and therefore, the thermal conductivity of small-sized materials can be lower than that of their bulk values.

Recent studies have also led to significant advances in the understanding of thermal transport in amorphous polymers [15–24]. It has been found that thermal transport is dominated by intrachain axial conduction via covalent bonds, while the interchain van der Waals conduction is marginal [15,16]. Thermal conductivity can be significantly affected by chain conformation (i.e., spatial extent of chains) [15], chain length [17,24], interchain cross-links [18], spatial confinement or density [19], strain [20], angular bending [21], branching [22], kinks [23], etc. Despite these advances, several fundamental questions remain: Can the thermal conductivity of amorphous polymers be further reduced below their common amorphous limit by the size effect, as has been widely found in crystalline materials in past decades? What affects the propagating

*tianli.feng2011@gmail.com; fengt@ornl.gov
†shresthass@ornl.gov

distance of heat carriers in amorphous polymers? Aside from the size effect, how can we tune the thermal conductivity of amorphous polymers such as using electrochemical engineering, which usually consist of covalent bonds? Since the thermal conductivity of crystals was found to be subject to strong size effects, the use of nanoengineering to tune thermal conductivity by several orders of magnitude for various applications has grown over the past two decades [11–14]. The ability to tune the thermal conductivity of amorphous polymers holds promise in many applications as well.

In the past decade, great advances have been made in the understanding of thermal transport in amorphous materials [25–32], which is contributed by the propagation of unlocalized atomic vibrational waves (propagons or phonons), diffusion of unlocalized waves (diffusons), and hopping of localized vibrations (locons). The understanding of thermal transport in amorphous polymers, however, is still mainly based on Cahill's model, which assumes that thermal transport is dominated by the random walk of localized oscillators between nearest neighbors (∼Å) and does not have a size effect beyond about 1 nm [30,33]. The phonon mean free path is usually estimated at about 0.1–1 nm by classical kinetic theory [17,34–37], which indicates no size effect either. This model, however, does not provide insight into the spectrum of thermal transport, and thus, cannot give exact answers. Therefore, experimental attempts have been made to explore the possible size effect of amorphous polymers, but the unknown interfacial resistance between polymer films and the substrate has prevented a firm conclusion from being reached [38,39]. Compared with crystalline materials or amorphous inorganic materials, the simulation of amorphous polymers is extremely computationally demanding due to the long equilibrium time for large numbers of possible large systems with different chain conformations.

Here, by using molecular dynamics simulations, we explore the size effect of thermal conductivity of four amorphous polymers, namely, polystyrene (*a*-PS), polyethylene (*a*-PE), polypropylene (*a*-PP), and ethylene vinyl alcohol (*a*-EVOH). These polymers have experimental bulk thermal conductivities (κ) ranging from 0.15 to 0.48 $\mathrm{W\,m^{-1}\,K^{-1}}$ [40], which approximately cover the entire range of κ values of typical amorphous polymers. Studies described in the literature usually investigate the thermal transport mechanism of amorphous polymers by using one single type of polymer, e.g., the simplest polymer, polyethylene. However, this practice may not be robust enough to draw general conclusions on amorphous polymers. Therefore, we select four polymers that cover nearly the entire range of κ values of typical amorphous polymers. This more comprehensive approach not only enables us to identify common heat transport features in amorphous polymers, but also some unique mechanisms of certain groups of polymers.

II. METHODS AND MATERIALS

The chemical units and atomic structures of the four polymers studied, i.e., *a*-PS, *a*-PE, *a*-PP, and *a*-EVOH, are shown in Fig. 1(a). The primary focus of this paper is on *a*-PS, as its amorphous nature is well acknowledged and its thermal conductivity is among the lowest in polymers. The four polymers are all composed of ethylene chains ($\text{-CH}_2\text{-CH}_2\text{-}$), but with different dangling molecules, which are highlighted in red in Fig. 1(a). PE has no dangling molecule; EVOH has a partially dangling -OH, i.e., only a certain portion of $\text{-[CH}_2\text{-CH}_2\text{]-}$ segments are attached with an -OH (this portion is 73% for L171B grade and 64% for H171B grade); PP and PS have dangling -CH_3 and $\text{-C}_6\text{H}_5$, respectively. They are listed in order of dangling mass fraction from low to high. The four amorphous polymers are built from Monte Carlo simulations with an energy-minimization algorithm and then stabilized in MD simulations using an all-atom polymer consistent force field (PCFF). [41] We note that PE, EVOH, and PP allow various degrees of crystallinity in experimental samples,

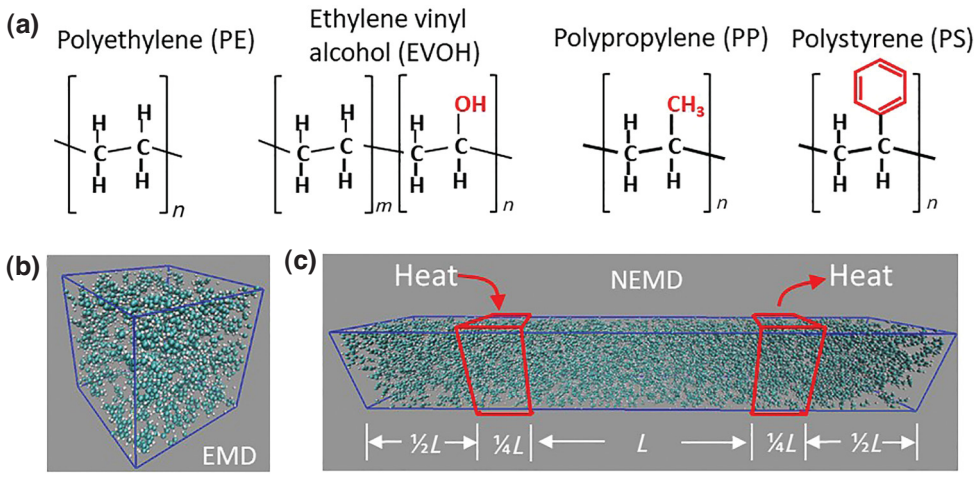

FIG. 1. Polymer molecular structures and simulation setups. (a) Monomers of PE, EVOH, PP, and PS. (b) Equilibrium molecular dynamics (EMD) and (c) nonequilibrium MD (NEMD) simulation setups. Periodic boundary conditions are applied along all three dimensions in both EMD and NEMD simulations.

but here we ensure random distortions for all polymers during construction to make amorphous forms. Statistical averages of thermal conductivities are taken from multiple different samples for each case study to avoid any artificial bias in constructing amorphous forms. In EVOH, the ethylene and vinyl alcohol molecules are randomly arranged in each chain. EVOH, PP, and PS are atactic, allowing the dangling molecules to randomly distribute on both sides of the polymer chain. The bulk and finite-size thermal conductivities are calculated using the Green-Kubo method based on equilibrium molecular dynamics (GKMD or EMD) and NEMD simulations with setups shown in Figs. 1(b) and 1(c), respectively. The simulation procedures are included in the Secs. S1 and S2 within the Supplemental Material [42], which includes Refs. [43–74].

III. RESULTS

A. Bulk thermal conductivity

We start by benchmarking the bulk thermal conductivities that we obtain through MD simulations with experimental and simulation data from the literature. MD simulations of the thermal conductivity of polymers have large fluctuations due to the flexible conformation (e.g., chain orientation, extension, and entanglement) and intrinsic statistical errors in MD with low thermal conductivity materials. Therefore, adequate independent simulations are required to obtain high-fidelity data. Our simulations indicate that the bulk thermal conductivities of *a*-PE, *a*-EVOH, *a*-PP, and *a*-PS at room temperature (i.e., 300 K) are 0.47 ± 0.02, 0.38–0.42 ± 0.02, 0.28 ± 0.02, and $0.16 \pm 0.02\ \mathrm{W\,m^{-1}\,K^{-1}}$, respectively, as shown in Table I. For EVOH, the thermal conductivity depends on the molar content of alcohol; thus, we obtain $0.38\ \mathrm{W\,m^{-1}\,K^{-1}}$ for $\mathrm{EVOH_{H171B}}$ (alcohol% = 64%) and $0.42\ \mathrm{W\,m^{-1}\,K^{-1}}$ for $\mathrm{EVOH_{L171B}}$ (alcohol% = 73%). Each κ value is the average of three to five random conformations, e.g., interchain entanglement and extension, with five independent simulations for each conformation. The values also include a convergence study with respect to the chain length that is discussed in Sec. III C. The four materials' thermal conductivities exhibit a decreasing trend with increasing dangling molecular weight fraction (or equivalently, decreasing backbone weight fraction), which supports the findings that the thermal conductivity of polymers is dominated by backbone transport along the chains [15,76,77]. This trend agrees with the recent finding by Luo *et al.* [22], although they only study how one-dimensional single-chain thermal conductivity changes using dangling molecules, while our work uses many entangled chains. Notably, the κ values that we obtain from EMD simulations agree reasonably well with the experimental data, 0.4–0.5, 0.3–0.33, 0.15–0.21, and $0.16\ \mathrm{W\,m^{-1}\,K^{-1}}$ for *a*-PE, *a*-EVOH, *a*-PP, and *a*-PS, respectively [40]. The small discrepancies are acceptable considering the nature of classical MD simulations, as well as the uncertainty in the sample quality and measurement techniques and instruments. Compared with simulations we find in the literature, which give values of 0.14–$0.21\ \mathrm{W\,m^{-1}\,K^{-1}}$ for *a*-PE [15,17,78], $0.07\ \mathrm{W\,m^{-1}\,K^{-1}}$ for *a*-PP [78], and 0.18–0.25 for *a*-PS [19,79] (no simulation data are found for EVOH in the literature), our simulation results are in better agreement with the experimental values. Reasons for our results agreeing better with experiments than the literature MD simulations might be (1) the PCFF potential can better predict the thermal transport properties in polymers than other potentials, and (2) the literature NEMD simulations have the size effect. Nonetheless, the absolute values of bulk κ do not significantly affect our study on the size effect, which only considers the relative change in κ with size.

TABLE I. Comparisons between amorphous polymers and inorganic semiconductors for their thermal conductivities and contributions of diffuson, locon, and propagon to thermal conductivity. Λ is the mean free path of the propagon. L_0 is the minimum thickness to ensure the amorphous nature of polymers.

		κ_{bulk} ($\mathrm{W\,m^{-1}\,K^{-1}}$)	Diffuson + Locon (%)	Propagon (%)	Λ (nm)	L_0 (nm)
MD simulations from this work (amorphous polymers)	*a*-PS	0.16 ± 0.02	84	16	~11.5	~5
	a-PE	0.47 ± 0.02	64	36	$\sim 70 \pm 32$*	~4.5
	a-PP	0.28 ± 0.02	64	36	$\sim 130 \pm 24$*	0.5–5
	a-EVOH	0.38–0.42	72	28	~0.2 (Λ_0)~38 (Λ_1)	...
Refs. (inorganic semiconductors)	Crystalline silicon [75]	150	~0	~100	~300	~0
	a-Silicon [46]	5	~22	~78	$\sim 1000 \pm 300$	~0
	a-Silica [47]	1.4	~100	~0	...	...

*Due to the slow increasing rate of the thermal conductivities of PE and PP with increasing thickness, the fitted mean free path might have a relatively large uncertainty.

B. Large size effect and long mean free path of propagons

1. Amorphous polystyrene

To explore the size effect of thermal transport in amorphous polymers, we start with *a*-PS, as its amorphous nature is well known and its size effect is of significant interest, especially in improving building insulation performance. We simulate the thermal conductivity of *a*-PS from $L = 0.5$ to 27 nm (beyond this length, the simulation becomes very difficult to converge, as the simulation domain is 2.5 times L). Notably, even for small L values (0.5–5 nm), we still keep the total simulation length longer than 10 nm to maintain the amorphous nature of *a*-PS. In this case, we assign a large portion of the simulation domain as heat reservoirs, so that the device length L can be shortened to any extent. The effect of reservoir length on the simulation results is avoided because we use the Langevin thermostat, which serves as an infinite-large thermal reservoir [44]. The simulation results are shown in Fig. 2(a). We find a strong size dependence that is not expected based on prevailing knowledge [30,33]. This size dependence is not monotonic and cannot be explained by phonon gas theory, as used in crystalline materials. To accurately describe the size-dependent thermal conductivity of crystalline materials, the phonon mode-resolved Boltzmann transport equation is required, which needs the broad-band mode-dependent phonon velocity, specific heat, and mean free path as inputs [46,80–83]. Often the phonon mean free path can spread over a broad range, for example, from 10 nm to tens of microns for silicon [46]. However, when these mode-dependent properties are not available, especially for complex solids, the gray Boltzmann transport equation with a gray phonon mean free path can still give reasonable and useful size-dependent thermal conductivity [66,84]:

$$\kappa(L) = \kappa_{\text{bulk}} \frac{1}{1 + \frac{4}{3}\frac{\Lambda}{L}}, \tag{1}$$

where Λ is the gray mean free path of heat carriers, i.e., phonons for crystals. L is the thickness of the material. k_{bulk} is the bulk thermal conductivity of the material, i.e., when its size is infinitely large. Here, this gray form of thermal conductivity is sufficient to interpret the MD simulation results of polymers. Notably, in the size-effect study and simulations, there is no Kapitza resistance [85] appearing in the systems, since there is no interface.

To understand size-dependent κ, we divide the size (thickness) range into several parts. (1) When the thickness is extremely small, e.g., 0–2.5 nm, the PS of interest does not have amorphous characteristics because it is composed of polymer chains connecting the hot and cold contacts throughout the film. In this case, the system is more like a crystalline structure, and heat can be conducted mainly through the backbones of single chains between hot and cold contacts, that is, heat transfer is dominated by intrachain conduction [18,86]. Therefore, the size-dependent κ of $L = 0$–2.5 nm is similar to the size effect of crystals, which is due to the ballistic effect [44,87,88], and this regime is referred as the "crystalline regime" in this work. (2) From $L = 2.5$ to 5 nm, all single PS chains are unable to connect the cold and hot contacts directly due to the torsion and entanglement, and interchain conduction becomes important. In this case, the PS can no longer be approximated by a crystalline system. It is not fully amorphous either, because it is not thick enough to allow a full amorphous chain conformation (e.g., torsion and entanglement). Therefore, we refer to $L = 2.5$–5 nm as a "transition regime from crystalline to amorphous" for *a*-PS. (3) Beyond 5 nm, the PS is fully amorphous, and this regime is of greatest interest in this work because we are exploring the nature of heat conduction in physically amorphous polymers, and it is also more practical than the other two regimes due to its fabrication feasibility. In this amorphous regime, heat is carried by diffusons, locons, and propagons (phonons). The first two conduction channels do not have size effects, and therefore, we propose to write the thermal conductivity as

$$\kappa(L) = \kappa_0 + \frac{\kappa_{\text{bulk}} - \kappa_0}{1 + \frac{4}{3}\frac{\Lambda - L_0}{L - L_0}}, \quad (L > L_0). \tag{2}$$

Here, κ_0 is the contribution of diffusons and locons, which has no size effect. The second term in Eq. (2) is the contribution of propagons, which has a size effect similar to phonons in crystals; therefore, Eq. (2) differs from Eq. (1) in that it introduces an additional quantity, L_0, to account for the starting thickness of the amorphous regime, giving the second term on the right side of Eq. (2). Therefore, Eq. (2) is referred to as a two-channel model that combines no size effect (i.e., difusons and locons) and size effect (i.e., propagons). The physical meaning of L_0 is the minimum thickness for a polymer to be called "amorphous," i.e., a film thinner than L_0 is partially crystalline. The value of L_0 for a polymer is the starting point of the amorphous regime that can be read from the trend of the size-dependent thermal conductivity, as shown in Fig. 2. For example, for *a*-PS, as shown in Fig. 2(a), L_0 is roughly estimated as 5 nm, which agrees reasonably well with the persistence length of polymers found in the literature [89]. κ_0 is the thermal conductivity when the size is L_0, which can also be read from the NEMD simulation results. κ_{bulk} is the bulk thermal conductivity obtained from EMD simulations in this work. For simplicity, we do not pursue a high accuracy of L_0 because it does not alter the overall physics, model, or trend. As

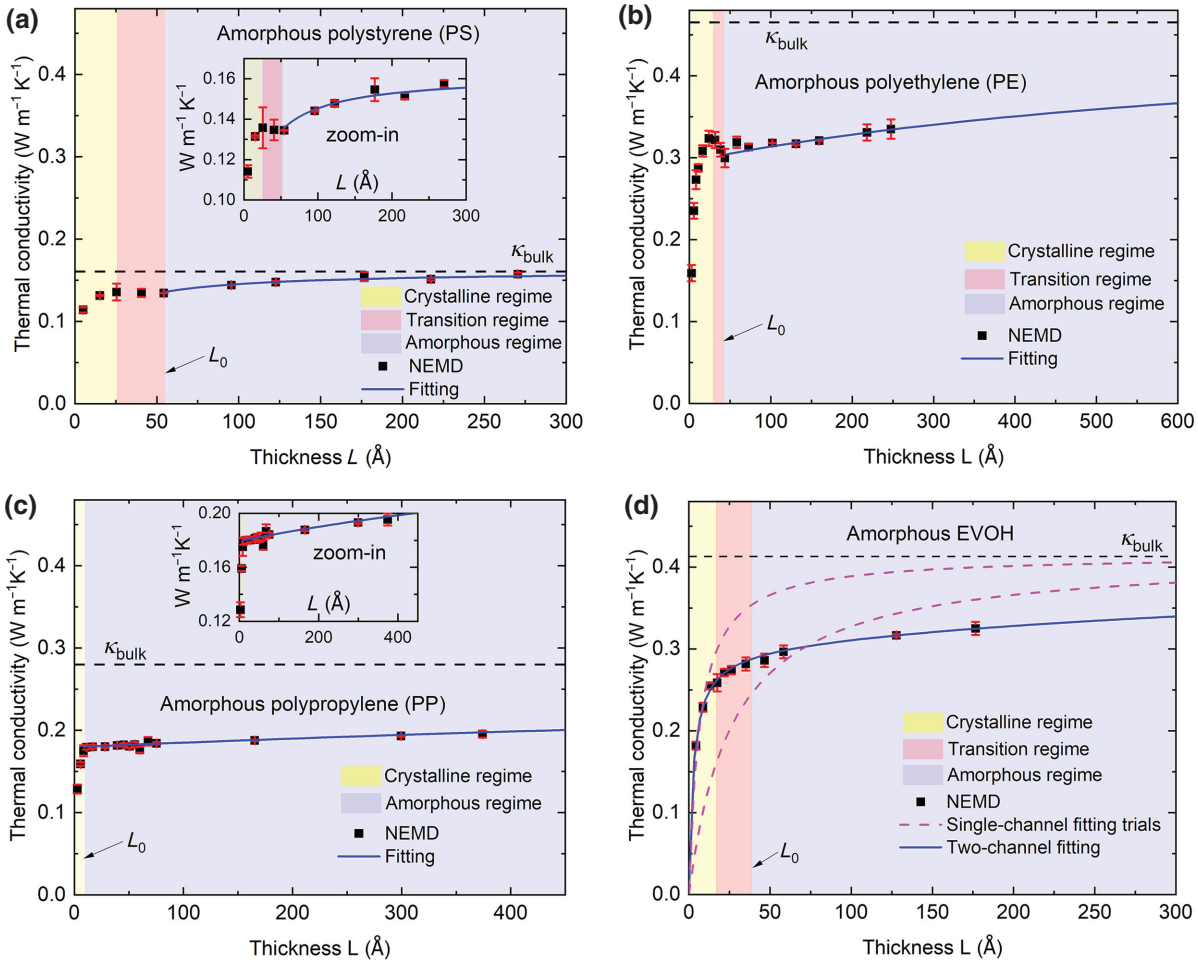

FIG. 2. Thickness-dependent thermal conductivity of (a) *a*-PS, (b) *a*-PE, (c) *a*-PP, and (d) *a*-EVOH films calculated by NEMD simulations at room temperature. Blue curves in (a)–(c) are fitted using Eq. (2) with Λas the only fitting parameter. In (d), green dashed curves and blue curve are fitted using Eqs. (1) and (3), respectively. Blue fitting curves in all figures will converge to bulk values (black dashed lines) at $L = \infty$. Differences between blue curves and bulk values at small L are the thermal conductivity contribution from propagons. Each NEMD data point is averaged among nine simulations, i.e., three independent NEMD simulations for three random structures. Error bars represent statistical errors of NEMD simulations. Insets in (a) and (c) are magnifications for clearer views of the size effect. Bulk values are obtained by EMD simulations in this work.

such, in Eq. (2), *there is only one fitting parameter*, Λ, the MFP of propagon, which is fitted as 11.5 nm, as shown in Table I for *a*-PS. The fitted curve agrees reasonably well with the NEMD data, demonstrating the feasibility of our model, Eq. (2). Notably, we randomly construct three different polymer structures for each L value to account for the uncertainty induced by local conformations of polymers. For each structure at each L value, we perform three independent NEMD simulations to account for the fluctuational nature of MD. As such, each data point in Fig. 2 is an average of nine independent NEMD simulations, which, at the same time, makes the study more computationally expensive than those for crystalline materials. The error bars represent the fluctuation of three MD simulations for each three random structures. Based on the relatively small error bars shown in Fig. 2(a), it is safe to claim that the size effect observed here is not due to an uncertainty of simulations. Our findings on the size effect of *a*-PS and the long MFP suggest a potential for further reducing the thermal conductivity for thermal insulation.

2. Amorphous polyethylene and polypropylene

To further examine whether the observed size effect of *a*-PS is a general trend in other amorphous polymers, we simulate the size-dependent thermal conductivity of *a*-PE, as shown in Fig. 2(b). A similar trend is observed in *a*-PE; that is, L can be divided into crystalline, crystalline-to-amorphous, and amorphous regimes based on the size-dependent thermal conductivity characteristics. With the model, Eq. (2), $\kappa(L)$ in the amorphous regime is fitted and the MFP of a propagon, Λ, of *a*-PE is obtained at around 70 nm. We acknowledge that the increasing trend of κ is

slow in the amorphous regime with L, and to have a better fitting, larger size simulations are required. However, due to the huge computational cost, we limit our simulations of *a*-PE to up to 17 nm, which compromises the quantitative interpretation of Λ being qualitative.

We also examine the size effect of *a*-PP, as shown in Fig. 2(c). Crystalline and amorphous regimes are clearly seen, while the transition regime is not clear, which may be between 0.5 and 5 nm. Nevertheless, to fit $\kappa(L)$ in the amorphous region using Eq. (2), we find that varying the value of L_0 from 0.5 to 5 nm does not affect the fitted results. The obtained MFP of a propagon in *a*-PP is about 130 nm.

Admittedly, the NEMD thermal conductivities of *a*-PE and *a*-PP at the studied thicknesses are still below the bulk value. However, for all polymers, we are not able to increase the simulation thickness anymore (the simulation domain is 2.5 times the film thickness) because a longer simulation domain will also require a larger cross section (otherwise the simulation is hard to converge), which will make the computational cost unaffordable. So, the thicknesses studied in Fig. 2 are nearly the maximum thicknesses we can run in NEMD simulations at this point in time. Here, we presume EMD and NEMD should give the same bulk thermal conductivity for polymers. Due to the slow increasing rate of the thermal conductivity of PE and PP, the fitted mean free path might have a relatively large uncertainty, which is noted in Table I.

3. *Amorphous EVOH*

The last polymer we examine is *a*-EVOH, which differs slightly from *a*-PS, *a*-PE, and *a*-PP in chemical composition by having additional oxygen atoms, in the form of hydroxyl groups (-OH). As shown in Fig. 2(d), we find similar characteristics for $\kappa(L)$ to those of the other three polymers; that is, $\kappa(L)$ cannot be fitted well by using the single-phonon model in Eq. (1). However, in *a*-EVOH, $\kappa(L)$ increases nearly smoothly with L and the transition between crystalline and amorphous regimes is not clear. Inspired by this, we combine Eqs. (1) and (2) by assuming two separate MFPs, Λ_0 and Λ_1, for crystalline phonons in the crystalline regime and propagons in the amorphous regime, respectively, and propose the following:

$$\kappa(L) = \kappa_{\text{bulk}} \left(\frac{f}{1 + \frac{4}{3}\frac{\Lambda_0}{L}} + \frac{1-f}{1 + \frac{4}{3}\frac{\Lambda_1}{L}} \right), \quad (L > 0). \quad (3)$$

The first term in parentheses in Eq. (3) represents short crystalline phonons through backbones, and the second term represents long propagons through van der Waals interactions. f, Λ_0, and Λ_1 are the fitting parameters. We find that this model fits $\kappa(L)$ of *a*-EVOH very well, and Λ_0 and Λ_1 are fitted as 0.2 and 38 nm, respectively. The portion of propagon, 1–f, is about 28%. Based on the values of Λ_0 and Λ_1, we can roughly tell the three regimes, as shown in Fig. 2(d). From 0 to $10\Lambda_0$, i.e., 0 to 2 nm, the first crystalline phonon term in Eq. (3) dominates, indicating the crystalline regime. From $\Lambda_1/10$ to ∞, i.e., 3.8 nm to ∞, the second propagon term in Eq. (3) dominates, indicating the amorphous regime. Here, the factors 10 for $10\Lambda_0$ and 1/10 for $\Lambda_1/10$ are just arbitrary numbers representing "much larger" and "much smaller," respectively, providing an estimation of the relative importance of the two channels. The ranges of these regimes identified by Eq. (3) are similar, or in the same order of magnitude, to those found in the three other polymers, indicating the rationality of our model in Eq. (3). We expect the long phonon mean free path predicted in this work to be measured in experiments by using various techniques, such as the thermal grating method [90] and ultrafast optical spectroscopy [12], which can measure the spectral phonon mean free path.

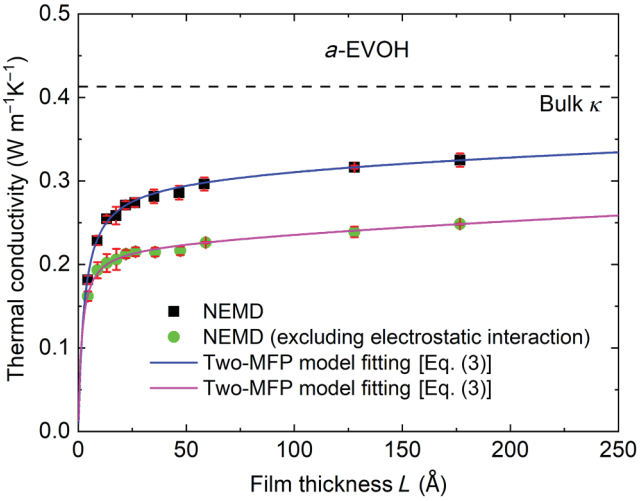

FIG. 3. Size-dependent thermal conductivities of *a*-EVOH with electrostatic interactions being included and arbitrarily excluded.

4. *Discussion*

The extracted propagon contribution to thermal conductivity and MFP in the various polymers studied is summarized in Table I. Propagons contribute to 16%, 36%, 36%, and 28% of the bulk thermal conductivity of *a*-PS, *a*-PE, *a*-PP, and *a*-EVOH, respectively. The results suggest a critical revisiting of the prevailing assumption of no size effect in amorphous polymers [30,33]. The obtained propagon MFPs of *a*-PS, *a*-PE, *a*-PP, and *a*-EVOH are around 11.5, 70, 130, and 38 nm, respectively. Although it is demonstrated that the phonon MFP spectrum along the axial direction of crystalline PE spreads about 1–1000 nm through first-principles calculations [91], the phonon MFP

of amorphous polymers is not expected to be much longer than 1 nm [38,39], and no size effect is expected. The long phonon MFP of amorphous polymers that we obtain indicates a critical review of the 0.1–1 nm values that usually assumed in the literature [17,34–37] based on classical kinetic theory, $\kappa = 1/3\, cv\Lambda$, where c and v are the specific heat and sound velocity, respectively. The kinetic model greatly underestimates the MFP by assuming all vibration modes have a sound velocity, while, in fact, most vibrational modes are optical and/or diffusive modes and have a much smaller velocity than that of the sound velocity [82,91,92]. This underestimation is also seen in crystals. For example, the effective phonon MFP of silicon is about 300 nm, while classical kinetic theory gives about 43 nm [75], and the latter is not able to predict well the size-dependent thermal conductivity. Notably, the MFP values shown in Table I are effective MFPs, and the actual MFP spectra in these polymers may spread over a wide range centered around the effective MFP value. Due to the amorphous nature of the polymers studied, the long phonon MFP is probably attributed to the van der Waals interaction. As found in the literature, van der Waals interactions can sustain long MFP phonons in crystalline materials [37,93]. The reason why amorphous and disordered materials can have a long phonon MFP might be that the long-wavelength phonons can barely see the local disorder, and therefore, can transport long distances with occasional scattering [46,94]. This phenomenon is also seen in defective crystals: the relative importance of long-wavelength phonons increases with an increasing concentration of defects [46,94] because the short-wavelength phonons are blocked by the defects. More importantly, it is also seen in amorphous inorganic materials: amorphous silicon (*a*-Si) has an effective MFP as long as 1000 nm [46] obtained by fitting the experimentally measured size-dependent thermal conductivity into Eq. (1), as seen in Fig. S3 within the Supplemental Material [42], which is much longer than the MFP of crystalline silicon.

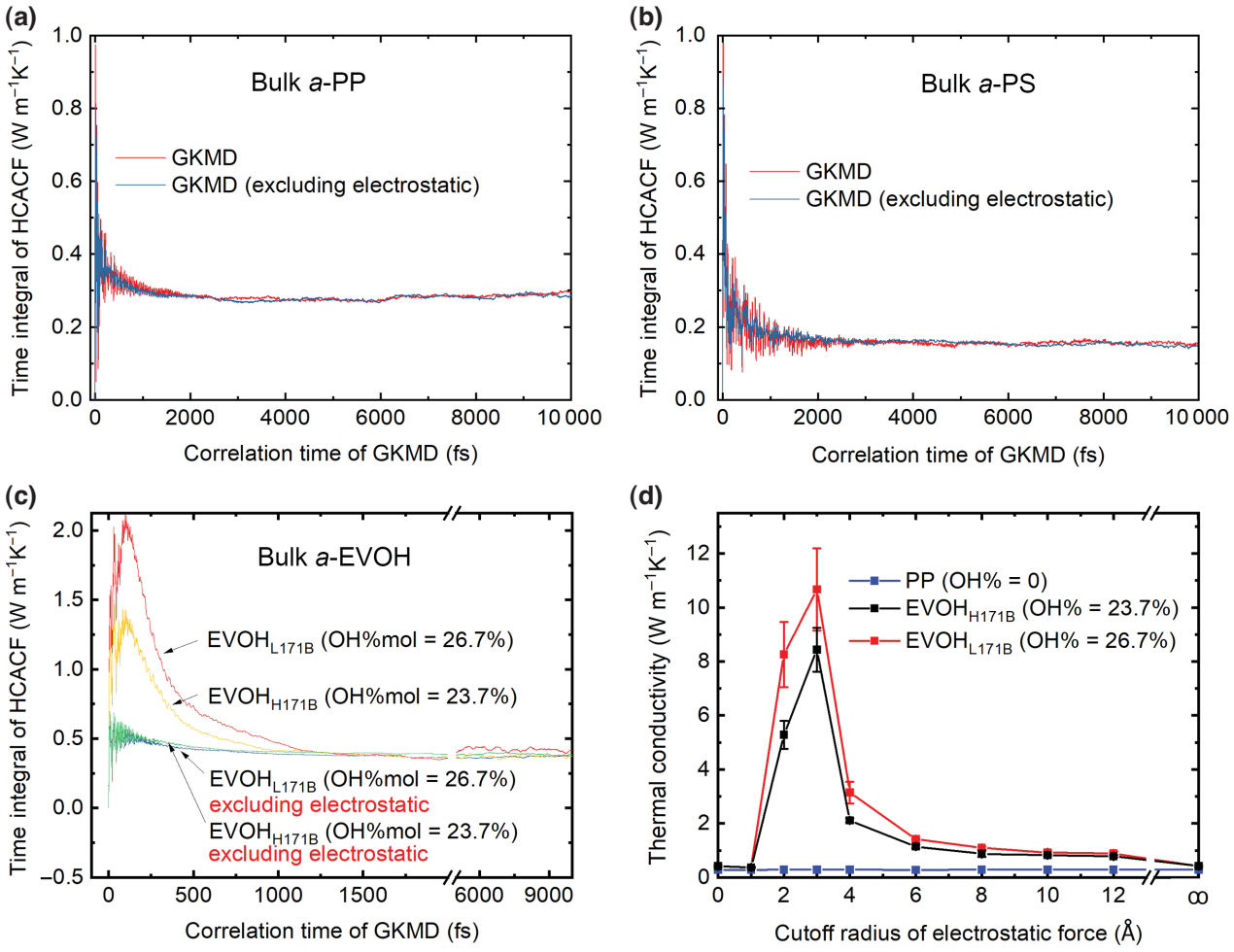

FIG. 4. Effect of electrostatic interactions on thermal conductivity of amorphous polymers. OH% is calculated by $n_O/(n_O + n_C)$. Without special notes, GKMD in this paper indicates that the electrostatic interaction is included and the cutoff radius is "infinity" by using the Ewald summation to account for long-range electrostatic interactions.

C. Intriguing effect of electrostatic potential

A comparison of the four polymers shows that *a*-PS and *a*-EVOH have the shortest phonon MFPs. The former is understandable because *a*-PS has a bulky dangling molecule (i.e., phenyl), which strongly reduces the phonon MFP and axial thermal conductivity of the ethylene chains [22]. However, the short MFP of *a*-EVOH is somewhat puzzling. The main difference between EVOH and the other polymers is that EVOH has oxygen atoms (in -OH), while the other three polymers are all composed of carbon and hydrogen. The existence of oxygen atoms induces a large electrostatic interaction because O-H has a much larger dipole moment than that of C-H. The net effective charge of oxygen in EVOH is $-0.56e$, while that of carbon in all four polymers is only about 0–0.1e, depending on the neighboring atoms, where e represents an elementary charge. To examine whether the electrostatic interaction shortens the phonon MFP, we simulate $\kappa(L)$ of EVOH via NEMD with electrostatic interactions being excluded arbitrarily. As shown in Fig. 3, the bulk κ remains the same, but $\kappa(L)$ becomes much smaller after the electrostatic interaction is excluded. The fitted phonon MFP, Λ_1 in Eq. (3), after excluding the electrostatic interactions is around 75 nm, which is much longer than that of the original value, 38 nm, before excluding electrostatic interactions. We then arbitrarily exclude the electrostatic interaction in *a*-PP and *a*-PS that are composed of carbon and hydrogen only, but changes to size-dependent κ are not observed (not shown in Fig. 3). These findings support our conjecture: it is the oxygen ions and electrostatic interaction that enhance $\kappa(L)$ and, therefore, reduce the size effect and phonon MFP in amorphous polymers. Notably, the phenomenon that electrostatic interactions increases $\kappa(L)$, while retaining κ(bulk), is only observed in EVOH and is not guaranteed for other polymers. We estimate that the electrostatic interactions retaining κ(bulk) in EVOH is just a coincidence, i.e., the following two factors that are discussed later in the following paragraphs compensate for each other: (1) electrostatic interactions have a trend of enhancing thermal transport by enhancing the interchain energy exchange, and (2) electrostatic interactions diminish the contributions of phonons by long-range anharmonic scattering. For other polymers, the electrostatic potential could have a much stronger effect on the bulk thermal conductivity. For example, a recent experiment shows that electrostatically engineered amorphous polymers can boost the thermal conductivity by about 10 times [95].

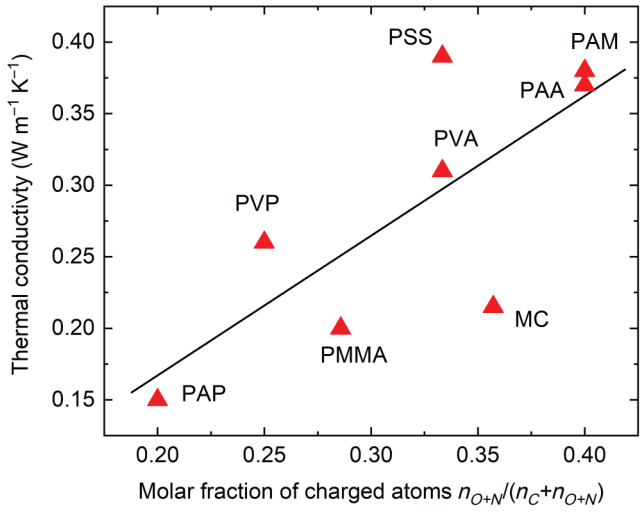

FIG. 5. Thermal conductivity of polymers measured in Ref. [96] as a function of the molar fraction of the charged atoms. They show a positive correlation with R^2 value of 0.574. Notably, they do not exactly follow a linear relationship because the various polymers have different physical properties, such as bulk modulus, sound velocity, heat capacity, and density, which significantly affect the thermal transport. Regardless of these physical properties, the positive correlation between the molar fraction of charged atoms and thermal conductivity can demonstrate the crucial role of electrostatic potential in determining the thermal conductivity of these materials. In these polymers, the charged atoms are oxygen and nitrogen. Here, carbon is treated as noncharged atom because its charge is negligible compared with those of oxygen and nitrogen. All hydrogen atoms are affiliated with carbon, nitrogen, and oxygen, and therefore, are not counted in this scheme. In addition, hydrogen contributes little to the thermal transport due to its high frequency and its dangling role.

We find that the decrease in the size effect by the inclusion of oxygen is not only seen in polymers, but also in inorganic materials. For instance, *a*-Si has a strong size effect, as previously discussed, but *a*-SiO_2 does not have a size effect, even down to 2 nm (see Sec. S3 within the Supplemental Material [42]) [47,72]. Similarly, *a*-Al_2O_3 does not show a size effect [72]. We suspect that it is the long-range anharmonic electrostatic interaction that diminishes the size effect in some inorganic oxides. This point is also supported by truncating the electrostatic interactions, as discussed in the following paragraphs. Notably, we do not compare the bulk thermal conductivities of *a*-Si and *a*-SiO_2, since the bulk thermal conductivity of a material is determined by many factors, including the chemical species, bonding strengths, sound velocities, and atomic masses, which cannot be predicted by electrostatic interactions only. Here, we only do self-consistent comparisons by comparing Si with Si itself with difference sizes, and we compare SiO_2 with SiO_2 itself with different sizes. For example, since *a*-Si does not have electrostatic interactions in it, it has large size effect. *a*-SiO_2 has strong electrostatic interactions in it, so it has a small, essentially no, size effect. Notably, *a*-Si has been well studied and its thermal conductivity is found to have significant contributions from phonons with a long mean free path. Here, we conjecture that the existence of long mean free path phonons in

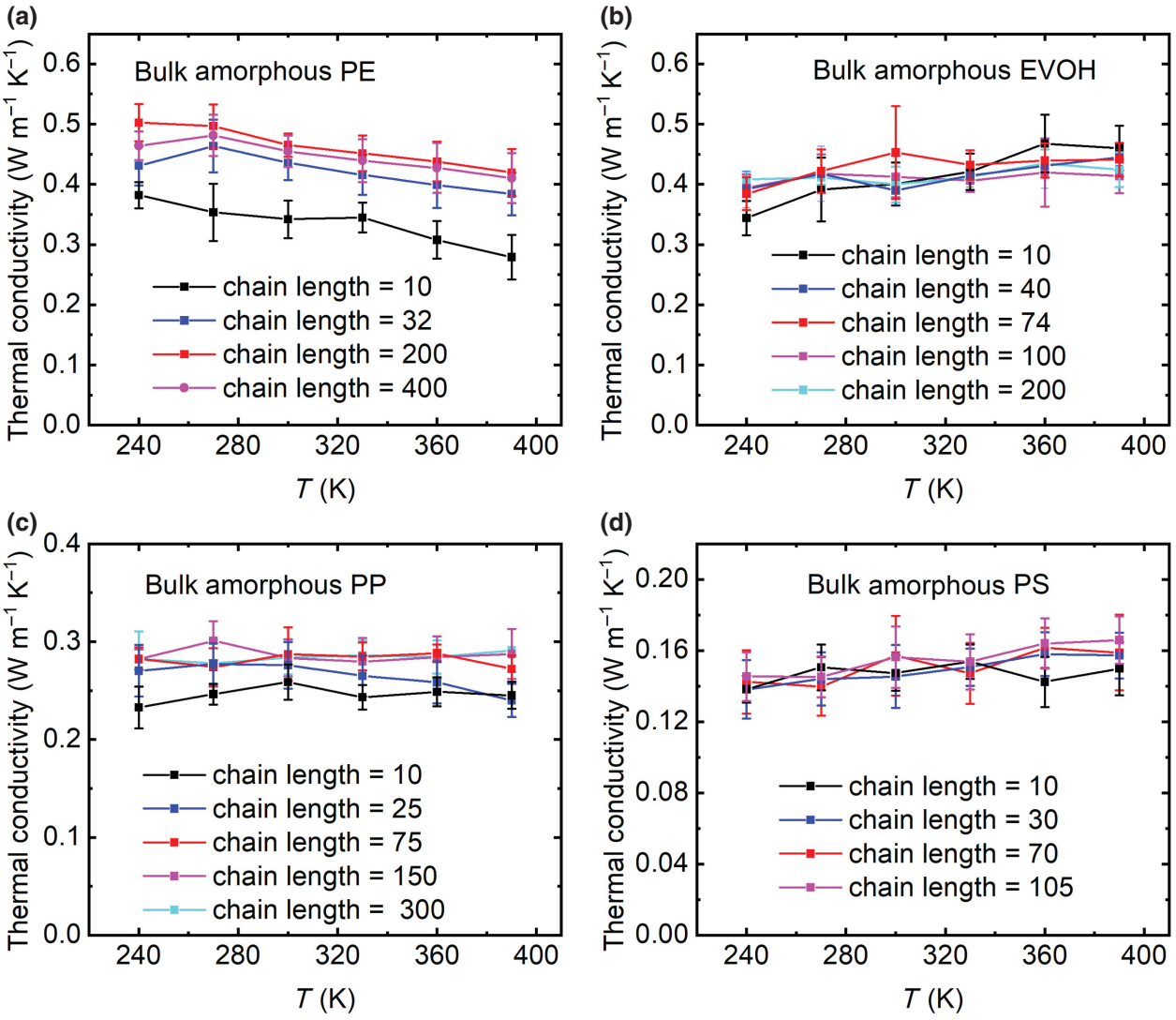

FIG. 6. Temperature-dependent thermal conductivities of bulk amorphous PE, EVOH, PP, and PS as a function of chain length.

a-Si might be partially because of the lack of electrostatic interactions. Nevertheless, the size effect of a material is determined by many factors, including sound velocities, anharmonicities, disorders, and interaction types, and it is irrational to determine the size effect solely on electrostatic interactions. Here, we take Si and SiO_2 as examples and propose ideas that might be examined by a further deeper analysis.

To gain a further insight into the role of oxygen ions and electrostatic interactions in thermal transport in polymers, we compare the time integrals of heat current autocorrelation functions (HCACFs) of bulk amorphous polymers with the electrostatic interactions being included and excluded, as shown in Figs. 4(a)–4(c). HCACF is a measurement of the correlation of the heat pulse (i.e., thermal fluctuation) with itself after a certain time in a system. A stronger correlation in a material indicates a higher thermal conductivity in this material, that is, the heat pulses or thermal fluctuations can last longer before dissipation. Here, we compare *a*-PP, *a*-PS, and *a*-EVOH, which all have some dangling molecules on the polyethylene chains. Notably, the structure does not change when we turn off the electrostatic interactions for all polymers. We find that, for *a*-PP and *a*-PS, which are composed only of carbon and hydrogen, the integrals of HCACFs do not change significantly upon including or excluding the electrostatic potential. However, for *a*-EVOH, which contains oxygen atoms, the integral of HCACF grows significantly at a short time (100 fs) correlation after the electrostatic potential is turned on [Fig. 4(c)]. This sharp growth is even greater at higher oxygen molar concentrations when we compare $EVOH_{L171B}$ (OH = 26.7%) and $EVOH_{H171B}$ (OH = 23.7%). At a long time correlation, although this sharp growth gradually decreases, $EVOH_{L171B}$, which has

more oxygen, still exhibits a larger converged bulk thermal conductivity than that of $EVOH_{H171B}$. Therefore, we can conclude that the oxygen ions and electrostatic interactions can increase thermal conductivity and, in particular, boost the transient thermal conductivity. This conclusion agrees with recent experimental observations that electrostatically engineered amorphous polymers can boost thermal conductivity by about 10 times [95]. Moreover, by comparing polymers with varying amounts of oxygen, as reported in Ref. [96], we find that the thermal conductivity generally increases with increasing oxygen content, as shown in Fig. 5, regardless of other important properties for thermal transport, such as modulus and density, indicating the important role of electrostatic interactions in enhancing the thermal conductivity.

We also examine the effect of the truncation radius of electrostatic potential, as shown in Fig. 4(d). It is shown that the finite-range electrostatic potential can boost the thermal conductivity of EVOH by up to 30 times. This enhancement is also greater for $EVOH_{L171B}$ than that of $EVOH_{H171B}$, since the former has a higher oxygen content. The inclusion of long-range interactions, however, gradually diminishes this enhancement. We suspect that the long-wavelength propagons that can barely be scattered by the short-range disorder are scattered by the long-range anharmonic electrostatic interactions. This hypothesis is supported by the fact that the long-range strongly anharmonic Coulombic interactions significantly suppress the thermal conductivity of ionic crystals, which generally cause salts to have a much lower thermal conductivity than that of covalent crystals [97,98]. To summarize, electrostatic interactions have two competing effects on thermal transport: the trend is to increase the thermal conductivity by enhancing the interchain energy exchange, but this diminishes the contributions of long-wavelength-propagon thermal transport by long-range anharmonic scattering. The exact role of electrostatic interactions on atomic vibrational spectra and phonon transport remains elusive and it is worth further study in the future.

We now discuss other effects that may affect thermal transport. It is known that the thermal conductivity of polymers greatly depends on the conformation (chain entanglement and extension) and chain length [15,17]. To draw conclusions about the size effect in thermal conductivity, we need to exclude the effect of conformation and chain length. The first effect is naturally excluded by performing statistical averaging for random conformations. The second effect is studied systematically for the four polymers. Figure 6 shows the temperature-dependent bulk thermal conductivities of the polymers with various chain lengths (for a summary of converged κ, see Fig. 7). Each point is averaged among three random conformations, with five independent simulations for each conformation to minimize the statistical error. The thermal conductivity generally changes with increasing chain length and eventually converges. We find that the converging chain lengths are 200, 40, 75, and 30 units of -[C*R*-C*R*]- for *a*-PE, *a*-EVOH, *a*-PP, and *a*-PS, respectively, where *R* represents H or dangling molecules. These chain lengths are chosen for the NEMD study in this work. Although *a*-PE shows strong chain-length-dependent κ, in agreement with Ref. [17], the other three polymers do not. Since in experimental samples the average chain length is much longer than these values, here we choose chain lengths that are long enough to ensure that they have no effect in our size-effect study. In Fig. S6 within the Supplemental Material [42], κ decreases with temperature in *a*-PE, but increases with temperature for the other polymers. Notably, MD uses classical Boltzmann statistics, which only works well for high temperatures; therefore, the temperature-dependent quantities obtained by MD can provide only a qualitative analysis instead of quantitative interpretation. Nevertheless, these results indicate that the size effect discussed above is not a result of crystallinity; instead, it is the nature of amorphous polymers.

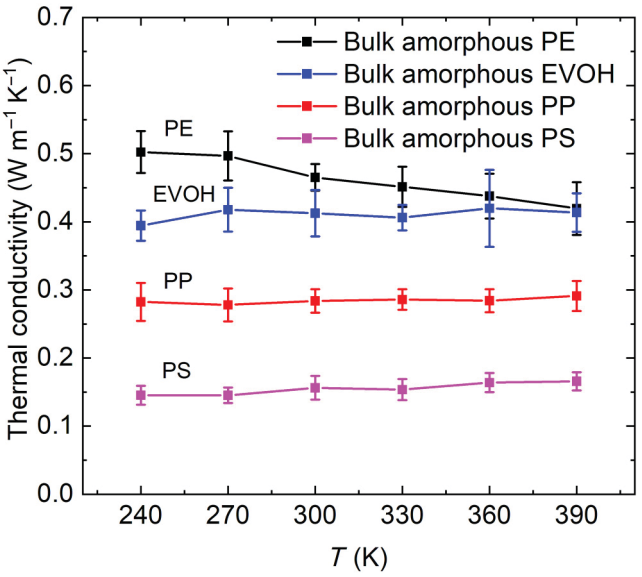

FIG. 7. Thermal conductivities of amorphous bulk PE, EVOH, PP, and PS as a function of temperature, as calculated by Green-Kubo MD.

IV. CONCLUSIONS

We find that the thermal conductivities of amorphous polymers can be further reduced below their bulk limit by 16% to 36% in the examples used in this study. This finding originates from the fact that the long-wavelength propagating heat carriers, i.e., phonons or propagons, can barely be scattered by the short-range disorder. A two-channel model that combines no size effect (i.e., difusons and locons) and size effect (i.e., propagons) is proposed to describe the size-dependent thermal conductivity.

We expect that the size effect we observe in four polymers, *a*-PS, *a*-PE, *a*-PP, and *a*-EVOH, generally occurs in amorphous polymers. We also find that the presence of -OH strongly enhances thermal transport by long-range electrostatic-interaction-facilitated energy exchange and reduces the size effect on thermal transport by scattering the long-wavelength phonons via long-range anharmonic Coulombic potential. We propose that the thermal conductivity of amorphous polymers is positively correlated with the concentration of charged atoms, such as oxygen and nitrogen atoms. Findings in this work will have a broad impact on the nano- and chemical engineering of polymers for various energy-related applications. We expect the size effect to be validated by future experiments with films on substrates.

ACKNOWLEDGMENTS

T.F., A.R., D.H., and S.S. acknowledge support from the project entitled "Models to Evaluate and Guide the Development of Low Thermal Conductivity Materials for Building Envelopes," funded by Building Technologies Office (BTO) of the Office of Energy Efficiency & Renewable Energy (EERE) at the U.S. Department of Energy (DOE). J.H. and J.L. acknowledge financial support from NSF under the award number CBET 1943813 and from the North Carolina State University Faculty Research and Professional Development Fund. Computations are performed at the National Energy Research Scientific Computing Center (NERSC) and the Extreme Science and Engineering Discovery Environment (XSEDE). Computations also use resources of the Compute and Data Environment for Science (CADES) at Oak Ridge National Laboratory. ORNL is managed by UT-Battelle, LLC, under Contract No. DE-AC05-00OR22725 for the U.S. Department of Energy.

The authors declare no conflicts of interest.

[1] M. Peplow, The plastics revolution: How chemists Are pushing polymers to New limits, Nature **536**, 266 (2016).

[2] P.-C. Hsu, A. Y. Song, P. B. Catrysse, C. Liu, Y. Peng, J. Xie, S. Fan, and Y. Cui, Radiative human body cooling by nanoporous polyethylene textile, Science (80-.) **353**, 1019 (2016).

[3] D. Rus and M. T. Tolley, Design, fabrication and control of soft robots, Nature **521**, 467 (2015).

[4] A. Chortos, J. Liu, and Z. Bao, Pursuing prosthetic electronic skin, Nat. Mater. **15**, 937 (2016).

[5] Y. Xu, D. Kraemer, B. Song, Z. Jiang, J. Zhou, J. Loomis, J. Wang, M. Li, H. Ghasemi, X. Huang, X. Li, and G. Chen, Nanostructured polymer films with metal-like thermal conductivity, Nat. Commun. **10**, 1 (2019).

[6] O. Bubnova, Z. U. Khan, A. Malti, S. Braun, M. Fahlman, M. Berggren, and X. Crispin, Optimization of the thermoelectric figure of merit in the conducting polymer poly(3,4-ethylenedioxythiophene), Nat. Mater. **10**, 429 (2011).

[7] S. Shin, M. Yang, L. J. Guo, and H. Youn, Roll-to-Roll cohesive, coated, flexible, high-efficiency polymer light-emitting diodes utilizing ITO-free polymer anodes, Small **9**, 4036 (2013).

[8] W. Zhang, Z. Tu, J. Qian, S. Choudhury, L. A. Archer, and Y. Lu, Design principles of functional polymer separators for high-energy, metal-based batteries, Small **14**, 1703001 (2018).

[9] J. Zhang, J. Yang, T. Dong, M. Zhang, J. Chai, S. Dong, T. Wu, X. Zhou, and G. Cui, Aliphatic polycarbonate-based solid-state polymer electrolytes for advanced lithium batteries: Advances and perspective, Small **14**, 1800821 (2018).

[10] Y. Yao, J. Sun, X. Zeng, R. Sun, J.-B. Xu, and C.-P. Wong, Construction of 3D skeleton for polymer composites achieving a high thermal conductivity, Small **14**, 1704044 (2018).

[11] J.-K. Yu, S. Mitrovic, D. Tham, J. Varghese, and J. R. Heath, Reduction of thermal conductivity in phononic nanomesh structures, Nat. Nanotechnol. **5**, 718 (2010).

[12] Y. Hu, L. Zeng, A. J. Minnich, G. Dresselhaus, and Mildred S. Chen, Spectral mapping of thermal conductivity through nanoscale ballistic transport, Nat. Nanotechnol. **10**, 701 (2015).

[13] T.-K. Hsiao, H.-K. Chang, S.-C. Liou, M.-W. Chu, S.-C. Lee, and C.-W. Chang, Observation of room-temperature ballistic thermal conduction persisting over 8.3 μm in SiGe nanowires, Nat. Nanotechnol. **8**, 534 (2013).

[14] J. P. Heremans, M. S. Dresselhaus, L. E. Bell, and D. T. Morelli, When thermoelectrics reached the nanoscale, Nat. Nanotechnol. **8**, 471 (2013).

[15] T. Zhang and T. Luo, Role of chain morphology and stiffness in thermal conductivity of amorphous polymers, J. Phys. Chem. B **120**, 803 (2016).

[16] A. Henry and G. Chen, Anomalous heat conduction in polyethylene chains: Theory and molecular dynamics simulations, Phys. Rev. B **79**, 144305 (2009).

[17] X. Wei and T. Luo, Chain length effect on thermal transport in amorphous polymers and a structure–thermal conductivity relation, Phys. Chem. Chem. Phys. **21**, 15523 (2019).

[18] G. Kikugawa, T. G. Desai, P. Keblinski, and T. Ohara, Effect of crosslink formation on heat conduction in amorphous polymers, J. Appl. Phys. **114**, 034302 (2013).

[19] H. Ma and Z. Tian, Effects of polymer chain confinement on thermal conductivity of ultrathin amorphous polystyrene films, Appl. Phys. Lett. **107**, 073111 (2015).

[20] J. Liu and R. Yang, Tuning the thermal conductivity of polymers with mechanical strains, Phys. Rev. B **81**, 174122 (2010).

[21] H. Subramanyan, W. Zhang, J. He, K. Kim, X. Li, and J. Liu, Role of angular bending freedom in regulating thermal transport in polymers, J. Appl. Phys. **125**, 095104 (2019).

[22] D. Luo, C. Huang, and Z. Huang, Decreased thermal conductivity of polyethylene chain influenced by short chain branching, J. Heat Transfer **140**, 1 (2018).

[23] X. Duan, Z. Li, J. Liu, G. Chen, and X. Li, Roles of kink on the thermal transport in single polyethylene chains, J. Appl. Phys. **125**, 164303 (2019).

[24] J. Zhao, J.-W. Jiang, N. Wei, Y. Zhang, and T. Rabczuk, Thermal conductivity dependence on chain length in amorphous polymers, J. Appl. Phys. **113**, 184304 (2013).

[25] P. B. Allen and J. L. Feldman, Thermal conductivity of disordered harmonic solids, Phys. Rev. B **48**, 12581 (1993).

[26] J. M. Larkin and A. J. H. McGaughey, Thermal conductivity accumulation in amorphous silica and amorphous silicon, Phys. Rev. B **89**, 144303 (2014).

[27] A. Jagannathan, R. Orbach, and O. Entin-Wohlman, Thermal conductivity of amorphous solids above the plateau, Phys. Rev. B **35**, 4067 (1987).

[28] M. Park, I.-H. Lee, and Y.-S. Kim, Lattice thermal conductivity of crystalline and amorphous silicon with and without isotopic effects from the ballistic to diffusive thermal transport regime, J. Appl. Phys. **116**, 043514 (2014).

[29] W. Lv and A. Henry, Non-Negligible contributions to thermal conductivity from localized modes in amorphous silicon dioxide, Sci. Rep. **6**, 35720 (2016).

[30] D. G. Cahill, S. K. Watson, and R. O. Pohl, Lower limit to the thermal conductivity of disordered crystals, Phys. Rev. B **46**, 6131 (1992).

[31] K. Sääskilahti, J. Oksanen, J. Tulkki, A. J. H. McGaughey, and S. Volz, Vibrational mean free paths and thermal conductivity of amorphous silicon from Non-equilibrium molecular dynamics simulations, AIP Adv. **6**, 121904 (2016).

[32] A. France-Lanord, S. Merabia, T. Albaret, D. Lacroix, and K. Termentzidis, Thermal properties of amorphous/crystalline silicon superlattices, J. Phys. Condens. Matter **26**, 355801 (2014).

[33] P. Keblinski, *Modeling of Heat Transport in Polymers and Their Nanocomposites, in Handbook of Materials Modeling* (Springer International Publishing, Cham, 2018), pp. 1–23.

[34] C. L. Choy, Thermal conductivity of polymers, Polymer (Guildf) **18**, 984 (1977).

[35] W. Reese, Temperature dependence of the thermal conductivity of amorphous polymers: Polymethyl methacrylate, J. Appl. Phys. **37**, 3227 (1966).

[36] H. Ma and Z. Tian, Chain rotation significantly reduces thermal conductivity of single-chain polymers, J. Mater. Res. **34**, 126 (2019).

[37] J. He, K. Kim, Y. Wang, and J. Liu, Strain effects on the anisotropic thermal transport in crystalline polyethylene, Appl. Phys. Lett. **112**, 051907 (2018).

[38] J. Liu, *Thermal Transport in Nanostructured Polymers* (University of Colorado at Boulder, Boulder, Colorado, 2013).

[39] J. Liu, S. Ju, Y. Ding, and R. Yang, Size effect on the thermal conductivity of ultrathin polystyrene films, Appl. Phys. Lett. **104**, 153110 (2014).

[40] M. Biron, *Detailed Accounts of Thermoplastic Resins, in Thermoplastics and Thermoplastic Composites (Second Edition)* (Elsevier, 2013), pp. 189–714.

[41] H. Sun, S. J. Mumby, J. R. Maple, and A. T. Hagler, An Ab initio CFF93 All-atom force field for polycarbonates, J. Am. Chem. Soc. **116**, 2978 (1994).

[42] See the Supplemental Material at http://link.aps.org/supplemental/10.1103/PhysRevApplied.14.044023 for MD simulation details, the size effect of SiO_2, and the fitting of the size-dependent thermal conductivity of *a*-Si.

[43] S. Plimpton, Fast parallel algorithms for short-range molecular dynamics, J. Comput. Phys. **117**, 1 (1995).

[44] Y. Hu, T. Feng, X. Gu, Z. Fan, X. Wang, M. Lundstrom, S. S. Shrestha, and H. Bao, Unification of nonequilibrium molecular dynamics and the mode-resolved phonon boltzmann equation for thermal transport simulations, Phys. Rev. B **101**, 155308 (2020).

[45] A. J. Griffin, F. R. Brotzen, and P. J. Loos, Effect of thickness on the transverse thermal conductivity of thin dielectric films, J. Appl. Phys. **75**, 3761 (1994).

[46] K. T. Regner, D. P. Sellan, Z. Su, C. H. Amon, A. J. H. McGaughey, and J. a Malen, Broadband phonon mean free path contributions to thermal conductivity measured using frequency domain thermoreflectance, Nat. Commun. **4**, 1640 (2013).

[47] J. L. Braun, C. H. Baker, A. Giri, M. Elahi, K. Artyushkova, T. E. Beechem, P. M. Norris, Z. C. Leseman, J. T. Gaskins, and P. E. Hopkins, Size effects on the thermal conductivity of amorphous silicon thin films, Phys. Rev. B **93**, 140201 (2016).

[48] K. E. Goodson, M. I. Flik, L. T. Su, and D. A. Antoniadis, Annealing-Temperature dependence of the thermal conductivity of LPCVD silicon-dioxide layers, IEEE Electron Device Lett. **14**, 490 (1993).

[49] N. Nagasima, Structure analysis of silicon dioxide films formed by oxidation of silane, J. Appl. Phys. **43**, 3378 (1972).

[50] Y. S. Ju and K. E. Goodson, Process-Dependent thermal transport properties of silicon-dioxide films deposited using Low-pressure chemical vapor deposition, J. Appl. Phys. **85**, 7130 (1999).

[51] D. G. Cahill and T. H. Allen, Thermal conductivity of sputtered and evaporated SiO_2 and TiO_2 optical coatings, Appl. Phys. Lett. **65**, 309 (1994).

[52] K. E. Goodson and Y. S. Ju, Heat conduction in novel electronic films, Annu. Rev. Mater. Sci. **29**, 261 (1999).

[53] T. Yamane, N. Nagai, S. I. Katayama, and M. Todoki, Measurement of thermal conductivity of silicon dioxide thin films using a 3ω method, J. Appl. Phys. **91**, 9772 2002).

[54] D. G. Cahill, M. Katiyar, and J. R. Abelson, Thermal conductivity of a -Si:H thin films, Phys. Rev. B **50**, 6077 (1994).

[55] M. P. Allen and D. J. Tildesley, *Computer Simulation of Liquids* (Oxford university, New York, 1987).

[56] X. Liu, J. Feldman, D. Cahill, R. Crandall, N. Bernstein, D. Photiadis, M. Mehl, and D. Papaconstantopoulos, High Thermal Conductivity of a Hydrogenated Amorphous Silicon Film, Phys. Rev. Lett. **102**, 035901 (2009).

[57] H.-S. Yang, D. G. Cahill, X. Liu, J. L. Feldman, R. S. Crandall, B. A. Sperling, and J. R. Abelson, Anomalously high thermal conductivity of amorphous Si deposited by Hot-wire chemical vapor deposition, Phys. Rev. B **81**, 104203 (2010).

[58] L. Wieczorek, H. J. Goldsmid, and G. L. Paul, *Thermal Conductivity of Amorphous Films, in Thermal Conductivity 20* (Springer US, Boston, MA, 1989), pp. 235–241.

[59] B. S. W. Kuo, J. C. M. Li, and A. W. Schmid, Thermal conductivity and interface thermal resistance of Si film on Si substrate determined by photothermal displacement interferometry, Appl. Phys. A Solids Surfaces **55**, 289 (1992).
[60] H. Wada and T. Kamijoh, Thermal conductivity of amorphous silicon, Jpn. J. Appl. Phys. **35**, L648 (1996).
[61] S. Moon, M. Hatano, M. Lee, and C. P. Grigoropoulos, Thermal conductivity of amorphous silicon thin films, Int. J. Heat Mass Transf. **45**, 2439 (2002).
[62] B. Zink, R. Pietri, and F. Hellman, Thermal Conductivity and Specific Heat of Thin-Film Amorphous Silicon, Phys. Rev. Lett. **96**, 055902 (2006).
[63] H. J. Goldsmid, M. M. Kaila, and G. L. Paul, Thermal conductivity of amorphous silicon, Phys. Status Solidi **76**, K31 (1983).
[64] T. Zhan, Y. Xu, M. Goto, Y. Tanaka, R. Kato, M. Sasaki, and Y. Kagawa, Phonons with long mean free paths in A-Si and a-Ge, Appl. Phys. Lett. **104**, 071911 (2014).
[65] S. Volz, X. Feng, C. Fuentes, P. Guérin, and M. Jaouen, Thermal conductivity measurements of thin amorphous silicon films by scanning thermal microscopy, Int. J. Thermophys. **23**, 1645 (2002).
[66] J. Kaiser, T. Feng, J. Maassen, X. Wang, X. Ruan, and M. Lundstrom, Thermal transport at the nanoscale: A Fourier's Law vs. phonon boltzmann equation study, J. Appl. Phys. **121**, 044302 (2017).
[67] P. Ferrando-Villalba, A. F. Lopeandia, L. Abad, J. Llobet, M. Molina-Ruiz, G. Garcia, M. Gerbolès, F. X. Alvarez, A. R. Goñi, F. J. Muñoz-Pascual, and J. Rodríguez-Viejo, In-Plane thermal conductivity of Sub-20 Nm thick suspended mono-crystalline Si layers, Nanotechnology **25**, 185402 (2014).
[68] M. C. Wingert, S. Kwon, M. Hu, D. Poulikakos, J. Xiang, and R. Chen, Sub-Amorphous thermal conductivity in ultra-thin crystalline silicon nanotubes, Nano Lett. **15**, 2605 (2015).
[69] F. R. Brotzen, P. J. Loos, and D. P. Brady, Thermal conductivity of thin SiO_2 films, Thin Solid Films **207**, 197 (1992).
[70] H. A. Schafft, J. S. Suehle, and P. G. A. Mire, Thermal conductivity measurements of thin-film silicon dioxide, IEEE 1989 Int. Conf. Microelec. Test Struct. **2**, 121 (1989).
[71] J. C. Lambropoulos, M. R. Jolly, C. A. Amsden, S. E. Gilman, M. J. Sinicropi, D. Diakomihalis, and S. D. Jacobs, Thermal conductivity of dielectric thin films, J. Appl. Phys. **66**, 4230 (1989).
[72] M. C. Wingert, J. Zheng, S. Kwon, and R. Chen, Thermal transport in amorphous materials: A review, Semicond. Sci. Technol. **31**, 113003 (2016).
[73] K. E. Goodson, M. I. Flik, L. T. Su, and D. A. Antoniadis, Prediction and measurement of the thermal conductivity of amorphous dielectric layers, J. Heat Transfer **116**, 317 (1994).
[74] O. W. Käding, H. Skurk, and K. E. Goodson, Thermal conduction in metallized silicon-dioxide layers on silicon, Appl. Phys. Lett. **65**, 1629 (1994).
[75] Y. S. Ju and K. E. Goodson, Phonon scattering in silicon films with thickness of order 100 Nm, Appl. Phys. Lett. **74**, 3005 (1999).
[76] S. Shen, A. Henry, J. Tong, R. Zheng, and G. Chen, Polyethylene nanofibres with very high thermal conductivities, Nat. Nanotechnol. **5**, 251 (2010).
[77] A. Henry, G. Chen, S. J. Plimpton, and A. Thompson, 1D-to-3D transition of phonon heat conduction in polyethylene using molecular dynamics simulations, Phys. Rev. B **82**, 144308 (2010).
[78] X. Wei and T. Luo, The effect of the block ratio on the thermal conductivity of amorphous polyethylene-polypropylene (PE-PP) diblock copolymers, Phys. Chem. Chem. Phys. **20**, 20534 (2018).
[79] E. A. Algaer, M. Alaghemandi, M. C. Böhm, and F. Müller-Plathe, Anisotropy of the thermal conductivity of stretched amorphous polystyrene in supercritical carbon dioxide studied by reverse nonequilibrium molecular dynamics simulations, J. Phys. Chem. B **113**, 14596 (2009).
[80] A. McGaughey and M. Kaviany, Quantitative validation of the boltzmann transport equation phonon thermal conductivity model under the single-mode relaxation time approximation, Phys. Rev. B **69**, 094303 (2004).
[81] J. Turney, E. Landry, A. McGaughey, and C. Amon, Predicting phonon properties and thermal conductivity from anharmonic lattice dynamics calculations and molecular dynamics simulations, Phys. Rev. B **79**, 064301 (2009).
[82] T. Feng and X. Ruan, Prediction of spectral phonon mean free path and thermal conductivity with applications to thermoelectrics and thermal management: A review, J. Nanomater. **2014**, 1 (2014).
[83] D. A. Broido, M. Malorny, G. Birner, N. Mingo, and D. A. Stewart, Intrinsic lattice thermal conductivity of semiconductors from first principles, Appl. Phys. Lett. **91**, 231922 (2007).
[84] A. Majumdar, Microscale heat conduction in dielectric thin films, J. Heat Transfer **115**, 7 (1993).
[85] A. Giri, P. E. Hopkins, J. G. Wessel, and J. C. Duda, Kapitza resistance and the thermal conductivity of amorphous superlattices, J. Appl. Phys. **118**, 165303 (2015).
[86] X. Wei, T. Zhang, and T. Luo, Chain conformation-dependent thermal conductivity of amorphous polymer blends: The impact of inter- and intra-chain interactions, Phys. Chem. Chem. Phys. **18**, 32146 (2016).
[87] G. Chen, Nanoscale Energy Transport and Conversion: A Parallel Treatment of Electrons, Molecules, Phonons, and Photons (Oxford University Press, 2005).
[88] T. Feng, W. Yao, Z. Wang, J. Shi, C. Li, B. Cao, and X. Ruan, Spectral analysis of Non-equilibrium molecular dynamics: Spectral phonon temperature and phonon local Non-equilibrium in thin films and across interfaces, Phys. Rev. B **95**, 195202 (2017).
[89] Kuhn and Persistence Length of Polymers, Polym. Prop. Database, ?>http//Polymerdatabase.Com/Polymer%20physics/Lp%20Table.Html (n.d.).
[90] J. A. Johnson, A. A. Maznev, J. Cuffe, J. K. Eliason, A. J. Minnich, T. Kehoe, C. M. S. Torres, G. Chen, and K. A. Nelson, Direct Measurement of Room-Temperature Nondiffusive Thermal Transport Over Micron Distances in a Silicon Membrane, Phys. Rev. Lett. **110**, 025901 (2013).
[91] N. Shulumba, O. Hellman, and A. J. Minnich, Lattice Thermal Conductivity of Polyethylene Molecular Crystals From First-Principles Including Nuclear Quantum Effects, Phys. Rev. Lett. **119**, 185901 (2017).

[92] S. Shenogin, A. Bodapati, P. Keblinski, and A. J. H. McGaughey, Predicting the thermal conductivity of inorganic and polymeric glasses: The role of anharmonicity, J. Appl. Phys. **105**, 034906 (2009).

[93] Q. Fu, J. Yang, Y. Chen, D. Li, and D. Xu, Experimental evidence of very long intrinsic phonon mean free path along the C-axis of graphite, Appl. Phys. Lett. **106**, 031905 (2015).

[94] T. Feng, X. Ruan, Z. Ye, and B. Cao, Spectral phonon mean free path and thermal conductivity accumulation in defected graphene: The effects of defect type and concentration, Phys. Rev. B **91**, 224301 (2015).

[95] A. Shanker, C. Li, G.-H. Kim, D. Gidley, K. P. Pipe, and J. Kim, High thermal conductivity in electrostatically engineered amorphous polymers, Sci. Adv. **3**, e1700342 (2017).

[96] X. Xie, D. Li, T.-H. H. Tsai, J. Liu, P. V. Braun, and D. G. Cahill, Thermal conductivity, heat capacity, and elastic constants of water-soluble polymers and polymer blends, Macromolecules **49**, 972 (2016).

[97] A. Seko, A. Togo, H. Hayashi, K. Tsuda, L. Chaput, and I. Tanaka, Prediction of Low-Thermal-Conductivity Compounds with First-Principles Anharmonic Lattice-Dynamics Calculations and Bayesian Optimization, Phys. Rev. Lett. **115**, 205901 (2015).

[98] S. Lee, K. Esfarjani, T. Luo, J. Zhou, Z. Tian, and G. Chen, Resonant bonding leads to Low lattice thermal conductivity, Nat. Commun. **5**, 3525 (2014).